Applied Catalysis A: General 470 (2014) 72–80

Contents lists available at ScienceDirect

Applied Catalysis A: General

journal homepage: www.elsevier.com/locate/apcata

Catalytic conversion of ethyl acetate over faujasite zeolites

Thanh Khoa Phung[a], Maria Maddalena Carnasciali[b,c], Elisabetta Finocchio[a,c], Guido Busca[a,c,*]

[a] Dipartimento di Ingegneria Civile, Chimica e Ambientale, Università di Genova, P.le J.F. Kennedy 1, I-16129, Genova, Italy
[b] Dipartimento di Chimica e Chimica Industriale, Via Dodecaneso 31, I-16146, Genova, Italy
[c] INSTM, Unità di Ricerca di Genova, Via Dodecaneso 31, I-16146, Genova, Italy

ARTICLE INFO

Article history:
Received 6 May 2013
Received in revised form 14 October 2013
Accepted 17 October 2013
Available online xxx

Keywords:
Ethyl acetate
Zeolite catalysts
Lewis acidity
Brønsted acidity
Faujasite
Pyridine adsorption

ABSTRACT

The catalytic conversion of ethyl acetate (EA) has been investigated over faujasite zeolites NaX, USY and HY. Characterization using pyridine adsorption shows that Lewis acid sites only exist on NaX while both Brønsted and Lewis acid sites are evident on both HY and USY. Catalytic experiments were performed in gas phase from 473 K to 973 K at atmospheric pressure with 2.16 h^{-1} WHSV in nitrogen. Cracking of EA to ethene and acetic acid is the predominant primary reaction in all cases. As a successive step, ketonization and decomposition of acetic acid occur. Over protonic zeolites Brønsted acidity catalyzes further oligomerization of ethene and cyclization of the further products, that finally produce coke precursors. The low-alumina protonic zeolite USY shows the highest conversion at low temperature, reaching total conversion at 673 K. Protonic zeolites cover by coke and slowly deactivate progressively. Fresh NaX is the least active but its catalytic activity is more stable, significant deactivation starting only after 5 h on stream.

1. Introduction

Ethyl acetate is largely used as a solvent for cleaning, paint removal and coatings. It is manufactured industrially with different processes: the esterification of acetic acid with ethanol is mainly performed in the liquid phase in catalytic distillation processes using H_2SO_4 as catalyst [1]:

$$CH_3COOH + CH_3CH_2OH \rightarrow CH_3COOCH_2CH_3 + H_2O \quad (1)$$

The reaction of acetic acid with ethene is performed in the presence of Silica-supported $H_4SiW_{12}O_{40}$ heteropolyacid catalyst at 130–230 °C, 0.5–1.5 MPa, and C_2H_4/CH_3COOH molar ratio 5–15 [2]:

$$CH_3COOH + CH_2{=}CH_2 \rightarrow CH_3COOCH_2CH_3 \quad (2)$$

It can also be produced via Tishchenko reaction of acetaldehyde using aluminum triethoxide as catalyst [3]

$$2CH_3CHO \rightarrow CH_3COOCH_2CH_3 \quad (3)$$

A fourth process has been developed recently, based on the dehydrogenation of ethanol [4] likely realized on copper chromite catalysts at 20–30 bar [5].

$$2CH_3CH_2OH \rightarrow CH_3COOCH_2CH_3 + 2H_2 \quad (4)$$

A number of other routes, such as the oxidative dehydrogenation of ethanol over vanadium catalysts [6], the homologation of methyl acetate with CO over Ru-based homogeneous catalysts [7], the biotechnological conversion of ethanol [8], the indirect fermentation of glucose [9] and the heterogeneously catalyzed two phase esterification (reaction (1)) over zeolite catalysts [10] have also been investigated.

To such a complex synthetic chemistry, a complex conversion chemistry corresponds, in part based on the reverses of the previous reactions. Indeed, few data are reported in the literature concerning the conversion of esters on solid acid catalysts.

Our main interest in the chemistry of esters is related to our attempts to develop selective catalysts for converting vegetable oils to liquid fuels and for refining of bioils. In both cases esters should be decomposed allowing the deoxygenation of the liquid by the removal of CO_2. In particular, the conversion of triglycerides [11] has been investigated over many different catalysts. Acid zeolites such as H-faujasites were found to catalyze at quite high temperatures (>500 °C) the deep cracking of vegetable oils mainly producing hydrocarbon rich gaseous mixtures [12].

Additional interest for investigating the conversion of ethyl acetate on zeolite catalysts is related to the possibility to use esters

* Corresponding author at: Dipartimento di Ingegneria Civile, Chimica e Ambientale, Università di Genova, P.le J.F. Kennedy 1, I-16129, Genova, Italy.
Tel.: +39 010 353 6024; fax: +39 010 353 6028.
E-mail address: Guido.Busca@unige.it (G. Busca).

0926-860X/$ – see front matter © 2013 Elsevier B.V. All rights reserved.
http://dx.doi.org/10.1016/j.apcata.2013.10.028

Table 1
The properties of investigated catalysts.

Zeolite sample	Commercial name	Source	Si/Al ratio	Na_2O (wt%)	Nominal cation form	Surface area (m^2/g)
NaX	Sylobead MS C 544	Grace	~1	–	Sodium	~500
HY	CBV 400	Zeolyst	2.55	2.8	Hydrogen	~700
USY	CBV 720	Zeolyst	15	0.03	Hydrogen	~750

as acylating agents in contact with acid catalysts [13] as well as to the reported application zeolite faujasite catalysts [14] for the abatement of ethyl acetate as a typical noxious polluting VOC [15].

In the previous research [16], we studied the conversion of ethyl acetate over Lewis acid alumina. To understand the effect of both Lewis and Brønsted acids, we investigated the conversion of ethyl acetate over three types of faujasite zeolites. We used NaX zeolite supposing to be a neutral, weak Lewis acid and weakly basic material, Al-poor USY supposed to be essentially Brønsted acidic only, and Al-rich HY supposed to be both Lewis and Brønsted acidic. We also performed an accurate surface characterization study to confirm such supposed properties. We will attempt to relate the catalytic behavior to the actual surface chemistry and acid/base properties of the catalysts.

2. Experimental

2.1. Catalytic materials

Three types of faujasite zeolites were investigated, whose properties are summarized in Tables 1 and 2. According to the information we have, Solybead MS C544 is a typical NaX adsorbent, Zeolyst CBV 400 is a typical HY zeolite while Zeolyst CBV 720, with small amount of Al, is essentially a Ultra Stable Y (USY) zeolite.

2.2. Gas phase catalytic ethyl-acetate conversion

The catalytic experiments were carried out at atmospheric pressure in a fixed-bed tubular quartz flow reactor, operating isothermally, loaded with 0.5 g of the catalyst (60–70 mesh sieved), and feeding 12.5% (v/v) ethyl acetate (EA) in nitrogen with 2.16 h^{-1} WHSV. The carrier gas (nitrogen) was passed through a bubbler containing high purity EA (99.5%). The temperature in the experiment was varied stepwise from 473 K to 973 K. Products were analyzed at each temperature after one hour running as from changing to desired temperature from previous temperature.

In order to study the deactivation phenomena on the catalyst, other experiments were performed as a function of time on stream using same conditions as above, at 623 K for HY and USY, 673 K for zeolite NaX. The reaction temperatures for this study have been chosen in order to have significant but uncomplete conversion of the reactant at the beginning.

EA conversion was defined as usual:

$$X_{EA} = \frac{n_{EA(in)} - n_{EA(out)}}{n_{EA(in)}}$$

while carbon selectivity to product i, S_i is defined as follows:

$$S_i = \frac{n_i}{n_i(n_{EA(in)} - n_{EA(out)})}$$

where n_i is the moles number of compound i, and ν_i is the ratio of stoichiometric reaction coefficients, corresponding also to the ratio between the number of carbon atoms in EA (i.e. 4) divided by the number of carbon atoms in the compound i.

The outlet gases were analyzed by a gas chromatograph (GC) Agilent 4890 equipped with a Varian capillary column "Molsieve 5A/Porabond A Tandem" and TCD and FID detectors in series. In order to identify the compounds of the outlet gases, a gas chromatography coupled with mass spectroscopy (GC-MS) Thermo Scientific with TG-SQC column (15 m × 0.25 mm × 0.25 μm) was used.

2.3. Infrared spectroscopy (IR) experiments

IR studies were done using Nicolet 380 FT-IR spectrometer. For IR skeletal studies the samples, including fresh and spent catalysts, were pressed into thin wafers with KBr and spectra where recorded in air. The acidity measurements were done by pyridine adsorption in an in situ IR-cell. The zeolite pure powders were pressed into thin wafers and activated in the IR cell connected with a conventional gas-manipulation apparatus at 773 K (for fresh catalysts) and 473 K (for spent catalysts) for 1 h. Gaseous pyridine (Py) was adsorbed at room temperature (p_{Py} ~1 Torr). After 15 min adsorption, pyridine was evacuated using high vacuum pump system (10^{-5} Torr), the IR spectra of the surface species were collected at adsorption time at room temperature and upon increasing temperature.

For EA infrared adsorption and reaction studies, pressed disks of the pure catalyst powders were activated "in situ" in the IR cell connected with a conventional gas-manipulation apparatus before any adsorption experiment. IR spectra of the surface species as well as of the gas phase were collected upon increasing temperature in static conditions (p_{EA} ~4 Torr).

The evaluation of the density of Lewis and Brønsted acid sites has been performed using the IR spectra of adsorbed pyridine according to Emeis [17].

2.4. Raman spectroscopy analysis

Raman spectra were collected over 3–5 mg of catalysts at room temperature on Renishaw microscope, performing at least 3 analyses at different positions and reducing the exposure to air for avoiding coke oxidation in case of spent catalysts. A laser of He–Ne was used at 632.8 nm focused on the sample by a microscope.

Table 2
Acidity of faujasite zeolites determined by IR-pyridine.

Samples	Brønsted acid sites (μmol/g)		Lewis acid sites (μmol/g)		Total acid sites (μmol/g)		Total acid sites		
	423 K	623 K	423 K	623 K	423 K	623 K	423 K	623 K	
NaX	0.0	0.0	758.8	107.6	758.8	107.6	0.11	0.015	mol_{py}/mol_{Na}
HY	301.2	111.0	229.3	64.7	530.5	175.8	0.12	0.04	mol_{py}/mol_{Al}
USY	164.8	103.0	99.9	62.8	264.7	165.8	0.25	0.16	mol_{py}/mol_{Al}

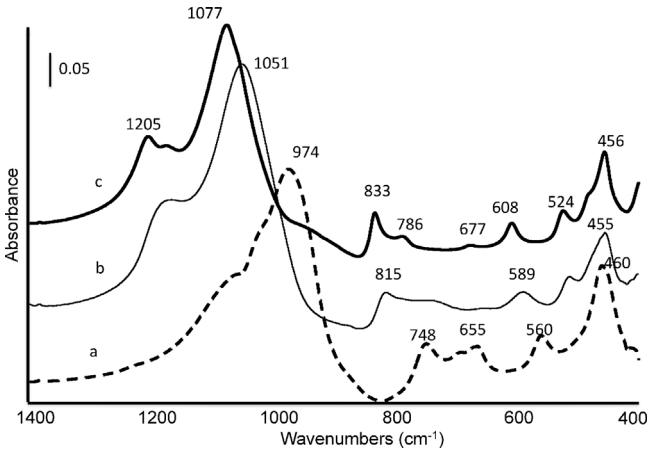

Fig. 1. FT-IR skeletal spectra (KBr pressed disks) of fresh (a) zeolite NaX, (b) zeolite HY, and (c) zeolite USY.

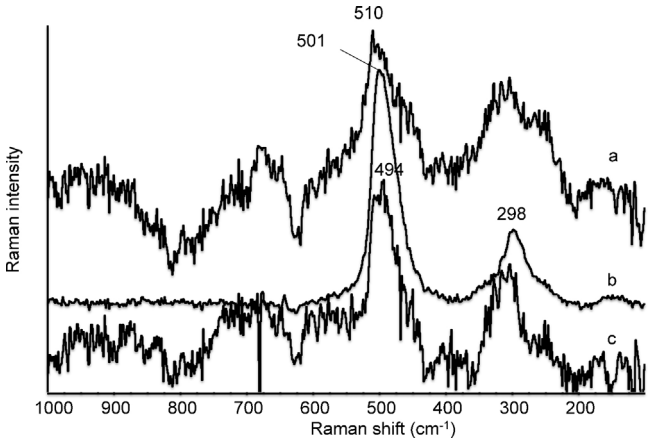

Fig. 2. Raman spectra of fresh faujasite zeolites that were performed at static condition at 600 cm^{-1}, 100 accumulations and 100% laser power of He–Ne laser at 632.8 nm: (a) zeolite NaX, (b) zeolite HY, and (c) zeolite USY.

3. Results and discussion

3.1. Catalyst skeletal characterization by vibrational spectroscopies

In Fig. 1 the skeletal IR spectra of the three fresh zeolite samples (KBr pressed disks) are reported. The strongest complex band observed in the 1300–900 cm^{-1} region is associated with the asymmetric stretching of the T—O—T bridges (ν1), where T are tetrahedrally coordinated Si or Al atoms [18,19]. This mode is slightly split because of coupling with the symmetric and asymmetric stretching of the four Si—O bonds of the SiO_4 octahedra. The actual position of the maximum and the shoulder is sensitive to the amount of Al ions in the framework, being typically shifted down the more, the higher the Al content is. The presence of Na ions interacting with the oxygen atoms of the T—O—T bridges may have an additional effect in lowering the position of these vibrational modes. This is in fact what we see in this work where the position of the main maximum is at 974 cm^{-1} for the NaX zeolite (Si/Al = 1), at 1051 cm^{-1} for the HY sample (Si/Al = 2.55) and at 1077 cm^{-1} for the USY sample (Si/Al = 15). Also the higher frequency components in the main band shift up in parallel up to 1205 cm^{-1} for USY, where actually two components are found. Due to the shift up of the main band, only in the case of the sample USY the broad and weak component due to Si—(OH) mode becomes apparent near 950 cm^{-1}.

The medium bands in the region 850–650 cm^{-1} are due essentially to a bending mode of the T—O—T bridges (ν2), although mixed with a symmetric stretching mode, which is split into two or three components. Also this complex mode shifts down the more the higher is the Al content, with the components at 833, 786 and 677 cm^{-1} for sample USY, at 815 and 734 cm^{-1} for sample HY and at 748, 692 and 665 cm^{-1} for sample NaX.

The lowest-frequency IR mode is associated with the out-of-plane deformation of the T—O—T bridges (ν3), i.e. it is a rocking mode. This mode is quite insensitive to the composition, being almost always observed at 465–450 cm^{-1}, intense.

Two other bands are observed between ν2 and ν3, and also shift with the same trend as ν1 and ν2, usually associated to modes strongly dependent on the structure of the zeolite: they are found at 608 and 524 cm^{-1} for USY, 589 and 514 cm^{-1} for HY, while for NaX the higher frequency one is observed at 560 cm^{-1} while the lower frequency one likely falls near 460 cm^{-1}, unresolved from ν3. Only for NaX bands an additional weak band is found at 403 cm^{-1}. This band, together with bands in the Far IR region (not shown here) at 368, 251, 185 and 106 cm^{-1} [19] are due to vibrational modes involving Na ions (Na—O stretchings).

In Fig. 2 the Raman spectrum of fresh faujasite zeolite catalysts is reported. Zeolite HY shows a strong peak at 501 cm^{-1} and a smaller one at 298 cm^{-1} in agreement with the published Raman spectra of HY zeolite samples [20,21]. The strongest Raman peak, which is assumed to be a T—O—T symmetric stretching mode coupled with a scissoring mode, is very sensitive to the structure of the zeolite, depending, in particular, from the size of the silicate rings. In the spectra of faujasites, its position near 500 cm^{-1}, is assumed to be associated to the presence of 4 membered rings [22]. The spectra of our other faujasite zeolites are much worst in quality, due to much stronger fluorescence. In any case they show too the strongest peak in the region near 500 cm^{-1}: the position of this peak seem to depend also on the framework Al content, but inversely than for the IR modes, being located at higher frequency in the case of NaX (510 cm^{-1}) in agreement with the literature [23–25] and at 494 cm^{-1} for the sample USY. Actually, we do not observe for the higher Si content sample the splitting of this mode, reported to be typical of highly siliceous faujasites [26].

3.2. IR study of the surface hydroxyl groups

In Fig. 3 the IR spectra of the three zeolites in the OH stretching region are reported. The spectrum of the catalyst USY clearly shows three OH stretching bands, at 3740 cm^{-1}, sharp and strong, 3627

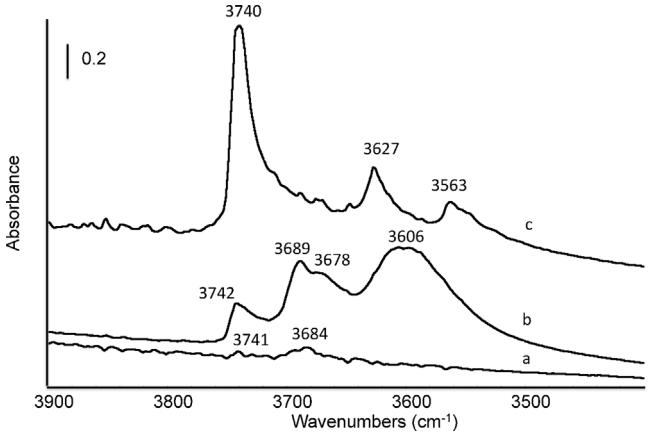

Fig. 3. FT-IR spectra of pure faujasite zeolites after activation at 773 K (νOH region): (a) zeolite NaX, (b) zeolite HY, and (c) zeolite USY.

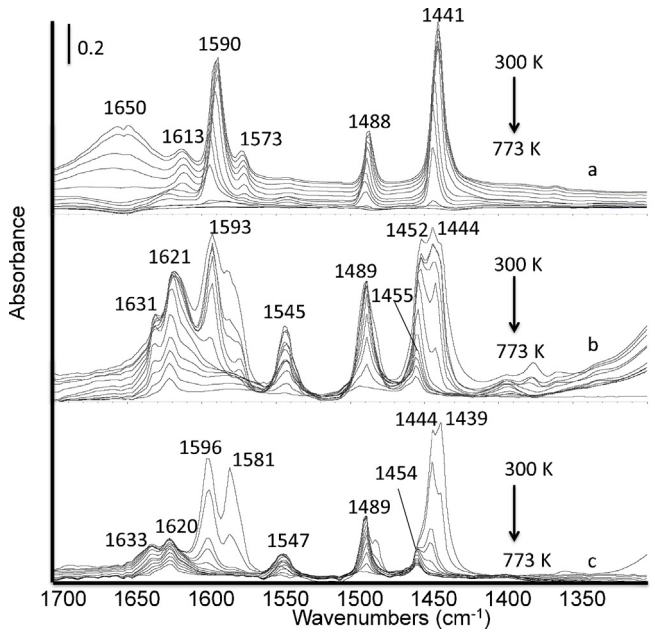

Fig. 4. FT-IR substraction spectra of the surface species arising from pyridine adsorbed on pure faujasite zeolites: (a) zeolite NaX, (b) zeolite HY, and (c) zeolite USY.

and 3563 cm^{-1}. Both lower frequency bands show components at their lower frequency sides. This spectrum is typical of ultrastable Y-type (USY) zeolites [27–29]. The strong band at 3740 cm^{-1} is assigned to νOH of free terminal silanols, located at the external surface. The other two peaks are attributed to the two main kinds of "structural" hydroxyl groups: the high frequency OH groups (HF) located in the supercages (3627 cm^{-1}), the low frequency OH groups (LF) located in the sodalite cages (3563 cm^{-1}). Their low frequency shoulders we observe near 3600 cm^{-1} and 3550 cm^{-1}, have been assigned to HF and LF species, respectively, interacting with residual extraframework (EF) species [30].

The spectrum of sample HY in the OH stretching region shows much weaker the band attributed to silanol groups, centered at 3742 cm^{-1}. It shows also a split band at 3689 and 3678 cm^{-1}, in the region usually assigned to OH groups located on extraframework material. Finally, a broad band is found at 3606 cm^{-1}, possibly with several components, in the region of zeolitic hydroxyl groups. This spectrum, where the distinction of the different zeolitic OHs is difficult, is quite typical of high Al content H-FAU zeolite [34].

The spectrum of the NaX sample shows, extremely weak, bands at 3741 and 3684 cm^{-1}. This suggests that an extremely small number of external silanol groups and OHs bonded to extraframework materials may exist. Instead, the bands due to bridging OHs, both in the supercage (HF) and in the sodalite cage (LF) appear to be fully absent. This indicates a full cationic exchange by sodium ions.

3.3. Surface acidity characterization by IR spectroscopy of adsorption of pyridine

The surface acidity of the three samples has been studied by IR spectroscopy, using pyridine as a probe molecule as reported in Fig. 4. The main adsorbed species on zeolite NaX are typically molecular: in fact the bands observed at 1590, 1573, 1488 and 1441 cm^{-1} are due to the 8a, 8b, 19a and 19b modes of molecular pyridine. The maxima of the sensitive 8a and 19b bands (1590 and 1441 cm^{-1}) are both slightly shifted up with respect to the liquid pyridine values of 1580 and 1438 cm^{-1} [32], showing interaction with a weak electron-withdrawing site.

By progressive outgassing, the 19b mode progressively decreases in intensity but its maximum progressively shifts up to 1444 cm^{-1}. On the other hand, the 8a mode is clearly complex, showing two main maxima at 1590 and 1613 cm^{-1}. By outgassing the former component decreases faster in intensity also shifting up to 1595 cm^{-1} while the latter decreases slower in intensity without a relevant shift, but disappears later leaving another weak residual band at definitely higher frequency (1622 cm^{-1}).

During the adsorption and desorption experiments a broad band also appears at 1650 cm^{-1}, that is associated to an absorption centered near 3450 cm^{-1}, in the OH stretching region. These features decrease progressively in intensity down to disappear by outgassing at 373 K (i.e. well before desorption of pyridine). They can be attributed to adsorbed water coming with pyridine vapour. Interestingly, when the bands of both molecular pyridine and water have disappeared, a weak band forms at 1546 cm^{-1} likely due to small traces of pyridinium ions (19a mode).

Thus we found three molecular pyridine species: the largely predominant species is certainly adsorbed on weakly Lewis acidic Na^+ cations, (8a and 19b bands at 1590–1595 cm^{-1} and 1441–1444 cm^{-1}, respectively), in agreement with previous studies [33]. Another less abundant species is bonded to stronger Lewis acid sites, i.e. highly exposed Na^+ ions, or Al^{3+} ions (8a band at 1613 cm^{-1}). A third molecular species (8a mode at 1622 cm^{-1}) is certainly associated to alumina or silica-alumina debris [34]. Additionally, traces of Brønsted sites are present or are formed during pyridine (and water) adsorption and desorption (19a mode of pyridinium ion at 1546 cm^{-1}).

The IR spectra of pyridine adsorbed on the two protonic zeolite samples, show, together with features due to adsorbed molecular pyridine, also bands associated to pyridinium ions, formed by protonation of pyridine on the Brønsted acid sites. The couple of bands at 1622–24 and 1452–55 cm^{-1} shows the existence, in both cases, of very strong Lewis acid sites typical of alumina and silica-alumina [34,35]. Pyridinium ions are mostly associated to bands at 1633–31 cm^{-1}, 8a, and 1545 cm^{-1}, 19a [36]. The relative intensities of the pyridinium ion and molecular pyridine bands, e.g. of the bands near 1633 cm^{-1} and near 1620 cm^{-1}, differ for the two protonic zeolites, showing a more pronounced role of Brønsted sites with respect to Lewis sites in the case of USY than for HY.

In Table 2, the results of the evaluation of the density of surface Lewis and Brønsted acid sites, based on pyridine adsorption experiments performed according to Emeis [17], are reported. The sites corresponding to pyridine species still adsorbed after outgassing at 423 K are assumed to be "total" sites, while those corresponding to pyridine species still found after outgassing at 623 K are assumed to be "strong" sites. Zeolite NaX shows only Lewis acid sites. According to the data, the zeolite NaX has more Lewis acid sites, also of the strong family, than protonic zeolites. It must be remarked, however, that, as shown by the IR spectrum of pyridine (8a vibrational mode), the "strong" Lewis sites on NaX are weaker than the "strong" Lewis sites on protonic zeolites, being mostly associated to Na^+ and Al^{3+} cations, respectively. In any case, the density of total (Lewis + Brønsted) strong acid sites follows the trend HY > USY > NaX. In case of protonic zeolites, HY contains much more Brønsted and Lewis acid sites than USY at 623 K, according to the higher concentration of Al ions, but total strong Brønsted and Lewis acid sites of both zeolites are similar.

The presence of Lewis sites on HY zeolite may be at least in part associated to the presence of extraframework (EF) material, evidence for whose existence is the band at 3698, 3678 cm^{-1} in the OH spectrum (Fig. 3) typically assigned to OH groups on EF. The presence of Lewis acid sites in the case of USY, instead, is not easily explained, taking into account the low concentration of Al in the framework and the lack of evidence of EF. We may note, however,

that the existence of active Lewis sites on USY has been reported previously [29,37,38].

The density of acid sites we calculate is actually low with respect to the Na and Al content in the catalytic materials (Table 2). We can mention, nevertheless, that we are measuring the number of sites still interacting with pyridine at 423 and 623 K, thus, taking into account the adsorption equilibrium, we have already freed part of the adsorption sites at this temperature. Additionally, in faujasites a significant part of sites are actually non accessible to large molecules being located in the sodalite cage and in the hexagonal prisms. In the case of Brønsted sites in protonic faujasites, only two of the four possible locations of the hydroxyl group point to the supercage [39] thus being accessible to pyridine. Moreover, in the case of HY extraframework alumina is present, thus reducing the number of Brønsted sites per Al ion. In the case of Na cations of NaX, structural data indicate that 66% of them are exposed in the supercage, although they can be not entirely accessible due to the high occupation of the cage. 33% of Na ions are certainly not accessible to pyridine, due to their location in the sodalite cage or in the hexagonal prism [40]. In any case, the density of Lewis and Brønsted sites we measure for HY and USY is consistent with those measured by other authors [37,38].

3.4. Catalytic conversion of ethyl acetate (EA)

In Fig. 5a the effect of temperature on conversions of EA is shown, while in Table 3 the data of product selectivities over the three zeolite catalysts are summarized. The conversion over a bed containing only silica glass, considered to be catalytically inactive, starts to be significant only above 700 K. With the zeolite catalysts, conversion is significant already at 473 K. The results obtained at 573 and 673 K, when conversion is high (>70%), are only considered for simplicity. Conversion obtained with zeolite NaX is the lowest, while that obtained with USY is the highest. The selectivity data obtained with NaX zeolite suggest that the following reaction sequence can occur at 673 K:
Cracking of ethyl acetate

$$CH_3COOC_2H_5 \rightarrow C_2H_4 + CH_3COOH \quad (5)$$

(i.e. the reverse of reaction (2)), and successive ketonization of the resulting acetic acid

$$2CH_3COOH \rightarrow CH_3COCH_3 + CO_2 + H_2O \quad (6)$$

In fact, ethene accounts for near 42% C selectivity on C-basis while the sum of acetic acid, CO_2 and acetone account for near 47% C selectivity, thus 89% C selectivity in total, with a number of heavy compounds as minor byproducts. When EA conversion approaches totality, at 723 K, the number of other byproducts increases, but the ketonization of acetic acid is complete, ethene/(CO_2 + acetone) C selectivity ratio being just near 1.

A possible alternative interpretation would be that ketonization of the ester occurs. In this case, the overall reaction should actually correspond to the sum of reactions (5)+(6). We opt for the first hypothesis (ketonization of acetic acid) due to the results of IR experiments (see below) and previous data on acetic acid conversion on alumina [16].

As further by-reactions, acetic acid decomposition

$$CH_3COOH \rightarrow CH_4 + CO_2 \quad (7)$$

and ethene dimerization

$$2C_2H_4 \rightarrow C_4H_8 \quad (8)$$

also occur to a small extent.

Over protonic zeolites the same products predominate, but the determination of the element balance is difficult, due to an excess of acetic acid (and its further conversion products) with respect to ethene, in particular at relatively low temperatures where conversion is still uncomplete, resulting also in an excess of oxygen in the products. This result could be explained by the production of heavy oligomeric species arising from the cationic polymerization of ethene, not revealed by our GC analysis. In fact, the carbon balance based on products revealed by GC is not fulfilled. Analyses were also performed with GC-MS revealing a number of heavy products (C atoms > 8) mostly mononuclear aromatic hydrocarbons with some weakly oxygenated compound, thus accounting for the lack of carbon balance. In parallel, deactivation phenomena seem to also appear, in particular over HY zeolite, where conversion at 723 K systematically drops to lower values with respect to the conversion observed at lower temperature. This suggests that heavy molecules can poison the catalyst active sites.

In order to study the stability of the activity of faujasite catalysts, the catalytic conversion of ethyl acetate with increasing time on stream at 623 K for HY and USY, 673 K for zeolite NaX has also been studied. The reaction temperatures for this study have been chosen in order to have significant but uncomplete conversion of the reactant at the beginning. As evident in Fig. 5b, the two protonic zeolites behave in a very similar way, and a progressive partial deactivation of both protonic catalysts is evident: after 7 h on stream at 623 K, the ethyl acetate conversion decreased from 87% to 45% for HY, 89% to 49% for USY. In contrast, the conversion on zeolite NaX at 673 K decreases slowly in the first 5 h from 78% to 72%, starting to drop only later.

In Table 4, the product selectivities analyzed upon deactivation experiments are reported. On NaX zeolite, selectivity to acetone + CO_2 + acetic acid is constant on time on stream very near 50%. In contrast, the selectivity to ethene starts near 45% and tends to decrease. In parallel, the selectivity to other products tends to increase, up to 16% after 7 h. Thus, deactivation of NaX seems to be associated to the progressive increase of active sites for ethene over-conversion, that produces more heavy products part of which should convert further into carbon species. A possible interpretation is that some kind of de-alumination and/or de-sodiation occurs, producing progressively more acidic, perhaps protonic, sites, that convert ethene into heavies and carbon precursors.

On HY, acetic acid selectivity is high on the fresh catalyst (near 60%) and, added to acetone and CO_2 selectivities, arrives to 65%, in agreement with low selectivity to ethene, 33%. Here, just the reverse occurs than before: selectivity to ethene + butene grows progressively up to above 45%, while selectivities to acetic acid, acetone and CO_2 go down to 52%. On USY a similar situation occurs, with higher final ethene selectivity (more than 50% including butene selectivity) and lower acetic acid, acetone and CO_2 selectivities (45%). This suggests that, in both cases, very acidic sites, probably of the Brønsted type, causing ethene over-conversion, are progressively coked.

3.5. IR study of the ethyl acetate conversion

Fig. 6 shows the IR spectra of the catalyst surface species during the EA conversion experiments performed in the IR cell on the three catalysts. After contact with EA vapour the spectra show features of molecularly adsorbed EA species (Table 5). These species are characterized by a shift down of the C=O stretching mode and a shift up of the C—O—C asymmetric stretching mode with respect to the liquid and gas phase EA species, as a result of interaction with electron withdrawing centers. In all cases, both intense bands due to C=O stretching and C—O—C asymmetric stretching of adsorbed EA are split, showing the presence of two different adsorbed species. By increasing reaction temperature additional species are formed.

It seems likely that the molecularly adsorbed EA species on NaX faujasite is mostly associated to interaction with Lewis acidic Na^+

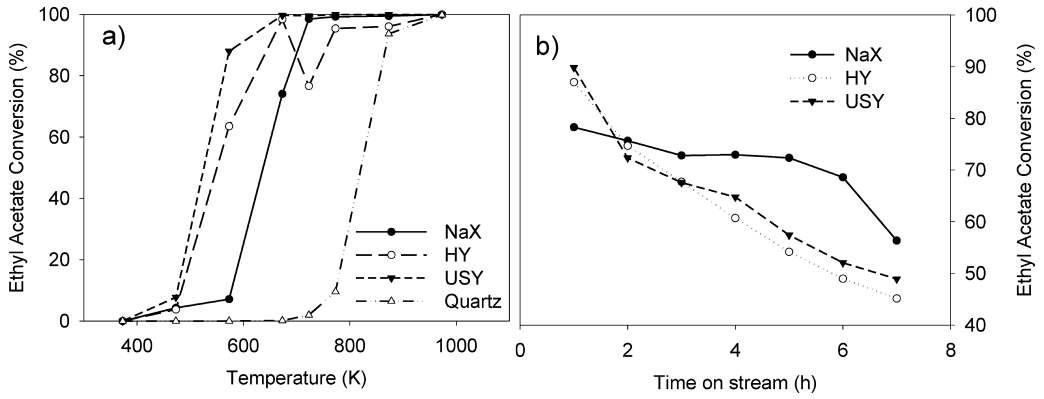

Fig. 5. Conversion of ethyl acetate (99.5%) at atmospheric pressure in a fixed-bed tubular quartz flow reactor with 2.16 h^{-1} WHSV in nitrogen (a) over 0.5 g of three faujasite zeolites and one silica glass as a function of reaction temperature from 473 K to 973 K and (b) over 0.5 g of three faujasite zeolites, at 623 K for HY and USY, at 673 K for zeolite NaX as a function of time on stream.

Table 3
Conversion (on C-basis) and selectivity to C-containing products of ethyl acetate over faujasite zeolites as a function of reaction temperature.

Catalyst	Temperature (K)	TC[a] (%)	Selectivity (%)							
			CH_4	CO	CO_2	C_2H_4	C_4H_8	CH_3COCH_3	CH_3COOH	Others
NaX	673	74.1	0.1	0.0	7.8	41.9	0.8	25.4	13.6	10.4
	723	98.5	0.5	0.2	12.5	36.0	2.1	24.5	0.3	23.9
HY	573	53.5	0.0	0.0	0.6	34.8	0.2	2.1	61.5	0.8
	673	98.4	0.1	0.6	4.3	30.5	2.3	11.3	47.8	3.2
	723	76.6	0.7	2.6	4.1	30.4	1.2	10.5	40.3	10.2
USY	573	88.0	0.0	0.0	1.0	24.8	0.5	2.9	70.4	0.4
	673	99.7	0.5	1.5	7.7	33.7	3.8	8.4	39.7	4.7
	723	99.5	3.6	7.6	12.6	47.8	7.9	6.2	8.2	6.0

Reaction using 0.5 g of the catalyst at atmospheric pressure with 2.16 h^{-1} WHSV in nitrogen.
[a] Total conversion based on carbon source (%).

cations. In fact, the spectrum observed is similar to that previously described for adsorption on alumina [16], with the most intense C=O stretching mode at slightly higher frequency than on alumina, due to the lower Lewis acidity of the predominant Na^+ cations of NaX with respect to Al^{3+} cations of alumina.

In the case of EA adsorption on protonic zeolites, it is evident that the surface hydroxyl groups are also involved. In fact over HY zeolite a strong band due to H-bonded OHs is observed at 3200 cm^{-1}, while on USY the maximum is observed near 3450 cm^{-1} with weak component at lower frequency. This parallels the predominance of

Table 4
Conversion (on C-basis) and selectivity to C-containing products of ethyl acetate over faujasite zeolites as a function of time on stream.

Catalyst	Time (h)	TC[a] (%)	Selectivity (%)							
			CH_4	CO	CO_2	C_2H_4	C_4H_8	CH_3COCH_3	CH_3COOH	Others
NaX at 673 K	1	78.3	0.0	0.0	18.7	45.3	1.4	27.0	0.0	7.6
	2	75.6	0.0	0.0	24.2	37.7	0.5	25.1	4.1	8.4
	3	72.8	0.0	0.0	21.4	37.6	1.2	25.7	4.7	9.5
	4	73.0	0.0	0.0	28.7	36.3	1.4	24.2	0.0	9.4
	5	72.4	0.0	0.0	25.1	36.9	0.8	25.7	0.0	11.6
	6	68.6	0.0	0.0	25.7	35.0	0.8	25.8	0.0	12.7
	7	56.3	0.0	0.0	25.5	31.5	0.8	25.9	0.0	16.3
HY at 623 K	1	87.0	0.0	0.0	1.8	33.5	0.7	4.7	58.7	0.5
	2	74.7	0.0	0.0	1.3	35.0	0.7	4.1	57.6	1.3
	3	67.7	0.0	0.0	1.3	38.5	0.8	3.7	54.0	1.6
	4	60.7	0.0	0.0	1.3	37.1	0.7	3.5	56.1	1.5
	5	54.2	0.0	0.0	1.1	40.8	0.7	3.5	51.6	2.3
	6	49.0	0.0	0.0	1.5	42.2	0.7	3.5	50.1	2.1
	7	45.1	0.0	0.0	1.8	44.5	0.7	3.3	47.3	2.3
USY at 623 K	1	89.8	0.0	0.0	3.3	40.6	1.7	5.8	48.6	0.0
	2	72.3	0.0	0.0	5.4	33.0	1.4	4.5	54.8	0.9
	3	67.6	0.0	0.0	7.4	36.8	1.6	4.2	47.7	2.3
	4	64.8	0.0	0.0	9.9	41.7	1.9	4.1	40.0	2.4
	5	57.4	0.0	0.0	2.0	42.0	1.8	4.2	47.3	2.7
	6	52.1	0.0	0.0	2.1	42.4	1.9	4.2	45.9	3.4
	7	48.9	0.0	0.0	2.4	48.7	2.8	4.4	38.8	2.9

Reaction using 0.5 g of the catalyst at atmospheric pressure with 2.16 h^{-1} WHSV in nitrogen, at 673 K for zeolite NaX, at 623 K for HY and USY
[a] Total conversion based on carbon source (%).

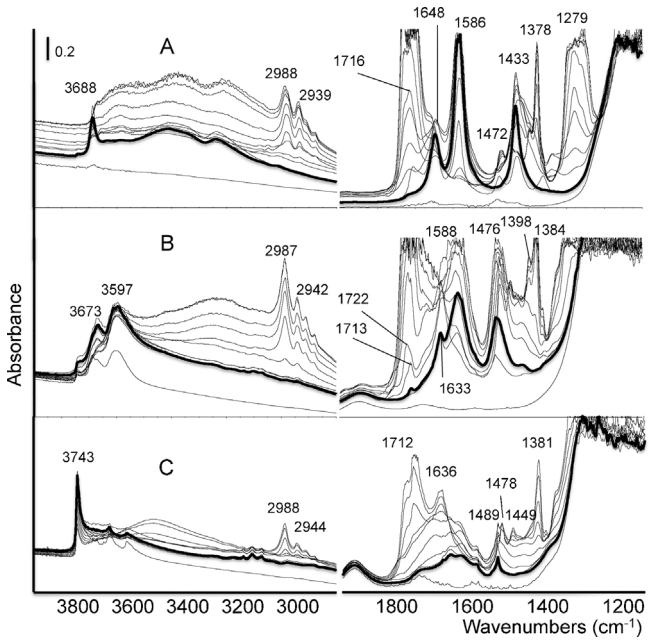

Fig. 6. FT-IR spectra of surface species arising from ethyl acetate adsorbed on faujasite zeolites after outgassing at 300 K and heating at increasing temperature in static vacuum (gas phase spectra subtracted): (a) zeolite NaX, (b) zeolite HY, and (c) zeolite USY.

weakly acidic external silanols (absorbing 3740 cm^{-1} over the latter catalyst), while in the former the strongly acidic zeolitic OHs absorbing near 3600 cm^{-1} predominate (see Fig. 3). The features of adsorbed EA on protonic zeolites do not differ very much from those observed on NaX and alumina, which is not really surprising because in both cases not only Brønsted acidic OH's are active, but also alumina-like Lewis acid sites. Thus molecular adsorption on electron-withdrawing centers through the carbonyl oxygen lone pair is thought to represent in all cases the first step in the catalytic reaction. On NaX the formation of absorption bands in the region 3700–3300 cm^{-1} may be due to some moisture coming with EA (as previously found on similar catalysts [41]) with the contribution of the proton left by acetic acid dissociation producing acetates.

The evolution of the surface (Fig. 6) and gas-phase species (Fig. 7) have been followed at increasing temperature by IR. In the three cases, the features of molecularly adsorbed EA decrease in intensity by increasing temperature. During this process, gas phase species appear, while, on the surface, bands of other species grow.

Over zeolite NaX the bands of adsorbed EA decrease progressively in intensity in the temperature range 473–673 K while, in the meanwhile, bands due to "stable" surface species grow near 1648, 1585 and 1435 cm^{-1}, with increasing intensity until 723 K, and decreasing intensity above this temperature.

At increasing temperature (from 523 K), gaseous reaction products appear, i.e. ethene (949 cm^{-1}; CH_2 wagging) and gaseous ethanol (C—O stretching at 1060 cm^{-1} and CH stretchings in the range 3000–2800 cm^{-1}). Acetic acid vapour is clearly evident at 573 K (bands at 1177 cm^{-1}, C—O symmetric stretching, 1293 cm^{-1}, C—O asymmetric stretching, 1794 cm^{-1}, C=O stretching). These data confirm the main reaction (5) observed in the flow reactor as the primary step, although ethanol may also be produced instead of ethene.

At higher temperature, from 623 K, ketene is made evident by the strong band at 2151 cm^{-1} (C=O stretching), most intense at 673 K when also methane appears (3015 cm^{-1} CH_4 stretching). By further increasing temperature, CO (C=O stretching at 2144 cm^{-1}) and CO_2 (O=C=O stretching at 2345 cm^{-1}) appear at 723 K. Thus showing two different decomposition paths of acetic acid, i.e. the above reaction (7) and the following reaction

$$CH_3COOH \rightarrow H_2C{=}C{=}O + H_2O \quad (9)$$

This reaction is indeed observed when acetic acid is adsorbed and heated on acidic surfaces such as alumina, where acetic acid ketonization also occurs [16]. Interestingly, no acetone is observed during IR experiment, while no ketene is observed in the flow reactor experiment. It is possible that ketene is the intermediate in acetone formation in agreement with previous studies [42]. Ketene may react producing acetone in the flow reactor experiment, due to the different conditions (higher concentration of reacting gas phase species).

$$CH_3COOH + H_2C{=}C{=}O \rightarrow H_3C\text{-}CO\text{-}CH_3 + CO_2 \quad (10)$$

This mechanism, however, contrasts the conclusions of Nagashima et al. [43]. Alternatively, ketene may combine with acetic acid to produce acetic anhydride [44]

$$CH_3COOH + H_2C{=}C{=}O \rightarrow (CH_3CO)_2O \quad (11)$$

which is revealed among the products in small amount by GC-MS, but cannot be found by IR, or decompose to produce ethene and CO

$$2H_2C{=}C{=}O \rightarrow C_2H_4 + 2CO \quad (12)$$

In the conditions where gaseous reaction products form, the bands of acetate species at 1586 and 1433 cm^{-1} grow, while they start to decrease only at higher temperature. This suggests that these species act essentially as spectators or even poisons during the reaction. The additional band at 1648 cm^{-1} is attributed to C=C stretching of precursors of carbon-like species, as it will be discussed below.

The spectra recorded during the same experiments performed on the two protonic zeolites are somehow similar to those described for the NaX zeolite. Over the HY catalyst the sequence of the formation of gas phase spectra is very similar, while the spectra of the adsorbed species are, relatively to those of adsorbed EA, more intense. The position of the bands is also different, ca. 1590 and 1476 cm^{-1} for acetate species, 1633 cm^{-1} with evident weak aromatic CH stretchings in the region 3000–3200 cm^{-1}. The spectrum of acetate species is quite similar to that of acetates on alumina [16], suggesting that they form over extraframework alumina debris. The quite weak feature at 1633 cm^{-1} and the weak but well evident CH stretchings in the region 3000–3200 cm^{-1} can be attributed to aromatic carbon deposits or olefinic precursors of such deposits.

Over USY the stability of the adsorbed species is far weaker, but the intensity of the band at 1636 cm^{-1} is relatively stronger and formed earlier than for the other catalysts. This band, however, disappears fast while the aromatic CH stretching bands persist, confirming that the band in the region 1650–1630 cm^{-1} is due to precursors of polyaromatic carbon species (C=C stretchings).

The catalytic data suggest that purely acidic catalysts, no matter if purely Lewis acidic or both Lewis and Brønsted acidic, behave in similar ways qualitatively, catalyzing first the cracking of the

Table 5
Vibrational frequency of ethyl acetate adsorbs on oxide catalysts by IR.

	Adsorbed ethyl acetate species			Other adsorbed species
	νC=O	δCH_3	νas C—O—C	
Gas	1764	1379	1243	
Alumina	1728, 1709	1401, 1379	1278, 1260	
USY	1729, 1712	1381		1640
HY	1720, 1712			1634, 1587, 1485
NaX	1727, 1713	1379	1279, 1255	1648, 1585, 1435

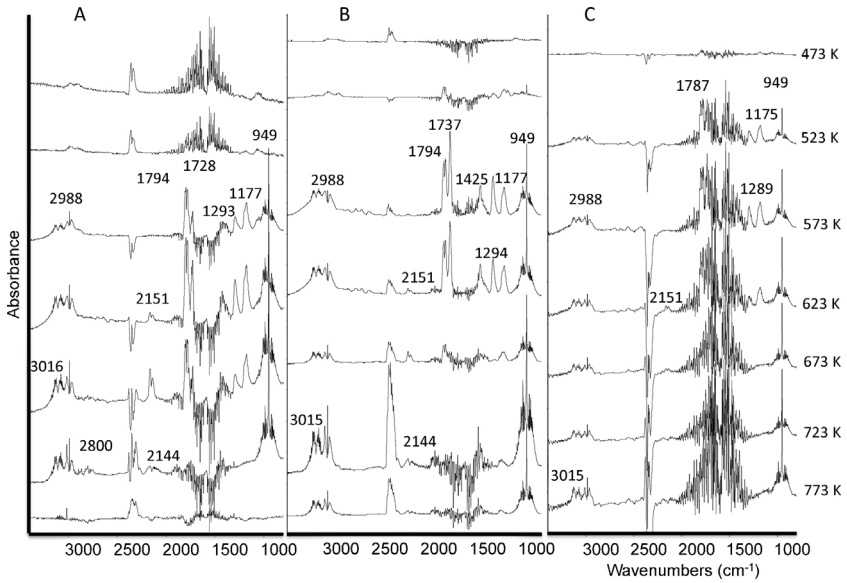

Fig. 7. FT-IR substraction spectra of the gas phase upon heating of ethyl acetate adsorbed on faujasite zeolites (the spectra obtained at a given temperature from which those obtained in the previous step (i.e. at 50 K less) were subtracted): (a) zeolite NaX, (b) zeolite HY, and (c) zeolite USY.

ester group, and (as a successive step) the ketonization of acetic acid. Brønsted acidic solids tend to catalyze also the successive oligomerization of ethene resulting in heavier compounds and more carbonaceous matter at the surface.

3.6. Studies on the spent catalyst HY

As reported before, deactivation phenomena appear to occur in EA conversion catalysis in particular with the HY catalyst, and carbonaceous deposits are formed in all cases. For this reason we investigated the catalysts after catalytic tests.

Raman spectra of the zeolites after reaction are reported in Fig. 8. Two strong peaks are observed, for the catalyst used at 723 K, at 1604 and 1368 cm^{-1}. The Raman peak observed near 1600 cm^{-1} over the three catalysts is likely the Raman active counterpart of the IR band observed at slightly higher frequency in the IR spectra reported in Fig. 6. They correspond to C=C stretching modes similar to those observed in the IR and Raman spectra of graphene and graphite [45–47]. The lower frequency band is also typically observed in the Raman spectra of coked zeolites and has also been assigned to polyaromatic coke structures [48]. Indeed a peak in a similar position is observed also in the spectra of diamond and carbon nanotubes [45,48]. Interestingly, the skeletal Raman peaks are almost disappeared also for the HY sample.

The IR spectra of the spent HY catalyst, discharged from the flow reactor and pressed, as such and after pyridine adsorption are shown in Fig. 9. Strong bands are observed on the catalyst, centered at ca. 1600 and 1480 cm^{-1}. These bands are similar to those were found on HY zeolite upon conversion of xylene [31] or on H-ZSM5 by coking with ethanol [49], attributed to polyaromatic compounds. The higher frequency component is again the IR active counterpart of the Raman mode observed in Fig. 8. IR spectra show that pyridine does not adsorb on the surface of spent zeolite HY: in fact no bands of adsorbed species are observed after contact with pyridine vapor. This shows that carbonaceous materials covered both Brønsted and Lewis acid sites of this catalyst.

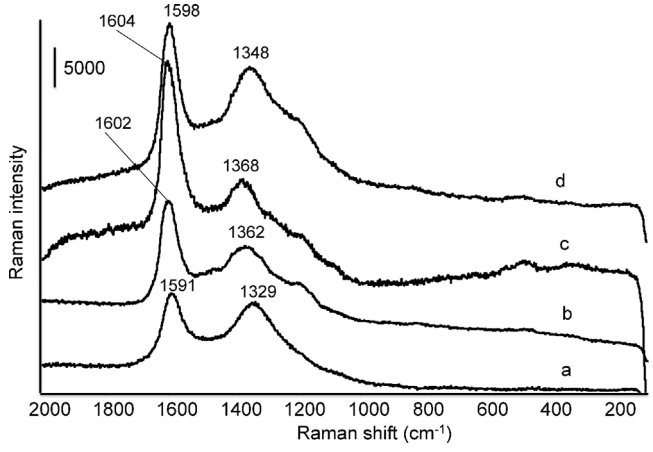

Fig. 8. Raman spectra of spent faujasite zeolites that were performed at extended condition at 2000–100 cm^{-1}, 4 accumulations and 10% laser power of He–Ne laser at 632.8 nm: (a) zeolite NaX at 973 K, (b) zeolite HY at 973 K, (c) zeolite HY at 723 K, and (d) zeolite USY at 973 K.

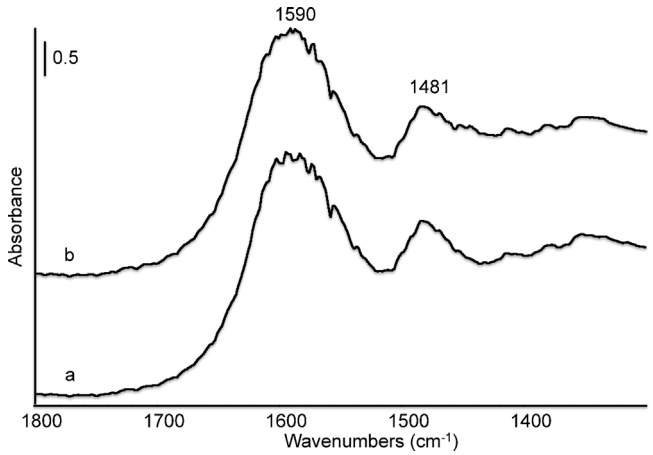

Fig. 9. FT-IR spectra of the surface species arising from pyridine adsorbed on spent zeolite HY reacted at 723 K: (a) spent HY and (b) adsorbed pyridine at room temperature.

4. Conclusions

In this paper the conversion of EA has been studied on three faujasite zeolites, supposed to be purely medium-strength Lewis acidic (NaX), purely strong Brønsted acidic (USY) and both Lewis and Brønsted acidic (HY). Actually, characterization experiments allowed us to emphasize the existence of strong Lewis acid sites, together with Brønsted acid sites, also on Al-poor USY. Additionally, some evidence of the presence of small amounts of "defect" strong Lewis sites (exposed Al ions) and also of Brønsted sites on NaX zeolites has also been obtained.

The acidic catalysts we investigated, no matter of their composition and of the nature of the acid sites, behave in similar way qualitatively, catalyzing first the cracking of the ester group, and (as a successive step) the ketonization of acetic acid. Brønsted acidic protonic zeolites tend to catalyze also the successive oligomerization of ethene resulting in heavier compounds, the formation of more carbonaceous matter at the surface and the progressive deactivation of the catalysts. The displaced deactivation of NaX is supposed to occur because of the progressive formation on stream of new acidic sites, possibly of the Brønsted type, finally producing coke.

In short, the lower conversion of EA over NaX zeolite is attributed to the lack of Brønsted sites. However, zeolite NaX, with only Lewis sites, might be a good catalyst to produce acetone from EA, better than HY and USY at the same temperature ($673\ K < T < 873\ K$). Also NaX is more stable than HY and USY, due again to the lack of Brønsted acidity which are main responsible for deactivation.

The data reported here find some parallelism with the triglycerides conversion over acidic catalysts [16]. Also in that case we can find, among the products, fatty acids and their ketonization products, together with acrolein coming from the glycerol chain. These are the products of the ester group cracking. However, comparison with those data also suggests that ethyl acetate reactivity only partially models triglycerides reactivity. In fact, in the case of triglycerides an additional reactivity occurs associated to the cracking of the glycerol chain, which induces more easy decarboxylation of the acid radicals into hydrocarbons (long chain paraffins and olefins). In the case of ethyl acetate the stability of the ethyl group to C—C bond cracking does not produce this chemistry. Studies of catalytic conversion of more complex esters can give further insights.

Acknowledgements

TKP acknowledges funding by EMMA in the framework of the EU Erasmus Mundus Action 2. EF acknowledges PRA2012 (University of Genova) for funding.

References

[1] I.-K. Lai, Y.-C. Liu, C.-C. Yu, M.-J. Lee, H.-P. Huang, Chem. Eng. Process. 47 (2008) 1831–1843.
[2] Y. Kamiya, T. Okuhara, M. Misono, A. Miyaji, K. Tsuji, T. Nakajo, Catal. Surv. Asia 12 (2008) 101–113.
[3] T. Seki, T. Nakajo, M. Onaka, Chem. Lett. 35 (2006) 824–829.
[4] S.W. Colley, J. Tabatabaei, K.C. Waugh, M.A. Wood, J. Catal. 236 (2005) 21–33.
[5] S.W. Colley, C.R. Fawcett, M. Sharich, M. Tuck, D.J. Watson, M.A. Wood, United States Patent, US 7,553,397, B1 (2009).
[6] B. Mehlomakulu, T.T.N. Nguyen, P. Delichère, E. van Steen, J.M.M. Millet, J. Catal. 289 (2012) 1–10.
[7] G. Braca, A.M.R. Galletti, G. Sbrana, F. Zanni, J. Mol. Catal. 34 (1986) 183–194.
[8] P. Christen, F. Domenech, J. Páca, S. Revah, Bioresour. Technol. 68 (1999) 193–195.
[9] C. de la Roza, A. Laca, L.A. Garcıía, M. Dı′az, Process Biochem. 8 (2003) 1451–1456.
[10] K.-C. Wu, Y.-W. Chen, Appl. Catal. A 257 (2004) 33–42.
[11] E. Sannita, B. Aliakbarian, A.A. Casazza, P. Perego, G. Busca, Renew. Sustain. Energy Rev. 16 (2012) 6455–6475.
[12] N. Taufiqurrahmi, A.R. Mohamed, S. Bhatia, Bioresour. Technol. 102 (2011) 10686–10694.
[13] G. Sartori, R. Maggi, Chem. Rev. 111 (2011) PR181–PR214.
[14] B. Silva, H. Figueiredo, O.S.G.P. Soares, M.F.R. Pereira, J.L. Figueiredo, A.E. Lewandowska, M.A. Bañares, I.C. Neves, T. Tavares, Appl. Catal. B 117–118 (2012) 406–413.
[15] T. Tsoncheva, G. Issa, T. Blasco, M. Dimitrov, M. Popova, S. Hernández, D. Kovacheva, G. Atanasova, J.M. López Nieto, Appl. Catal. A 453 (2013) 1–12.
[16] T.K. Phung, A.A. Casazza, B. Aliakbarian, E. Finocchio, P. Perego, G. Busca, Chem. Eng. J. 215–216 (2013) 838–848.
[17] C.A. Emeis, J. Catal. 141 (1993) 347–354.
[18] E. Astorino, J. Peri, R.J. Willey, G. Busca, J. Catal. 157 (1995) 482–500.
[19] G. Busca, C. Resini, in: R.A. Meyers (Ed.), Encyclopedia of Analytical Chemistry, Wiley, Chichester, 2000, pp. 10984–11020.
[20] C. Brémard, M. Lemaire, J. Phys. Chem. 97 (1993) 9695–9702.
[21] I. Halasz, M. Agarwal, B. Marcus, W.E. Cormier, Microporous Mesoporous Mater. 84 (2005) 318–331.
[22] A. Isambert, E. Angot, P. Hébert, J. Haines, C. Levelut, R. Le Parc, Y. Ohishi, S. Koharad, D.A. Keen, J. Mater. Chem. 18 (2008) 5746–5752.
[23] F. Roozeboom, H.E. Robson, S.S. Chan, Zeolites 3 (1983) 321–328.
[24] J. Twu, P.K. Dutta, C.T. Kresge, Zeolites 11 (1991) 672–679.
[25] Y. Liu, G. Xiong, C. Li, F.S. Xiao, Microporous Mesoporous Mater. 46 (2001) 23–34.
[26] P. Bornhauser, D. Bougeard, J. Raman Spectrosc. 32 (2001) 279–285.
[27] M.W. Anderson, J. Klinowski, Zeolites 6 (1986) 455–466.
[28] M. Sierka, U. Eichler, J. Datka, J.J. Sauer, J. Phys. Chem. B 102 (1998) 6397–6404.
[29] T. Montanari, E. Finocchio, G. Busca, J. Phys. Chem. C 115 (2011) 937–943.
[30] W. Daniell, N.-Y. Topsøe, H. Knözinger, Langmuir 17 (2001) 6233–6239.
[31] H.S. Cerqueira, P. Ayrault, J. Datka, M. Guisnet, Microporous Mesoporous Mater. 38 (2000) 197–205.
[32] T.D. Klots, Spectrochim. Acta Part A 54 (1998) 1481–1498.
[33] R. Ferwerda, J.H. van der Maas, P.J. Hendra, J. Phys. Chem. 97 (1993) 7331–7336.
[34] G. Busca, Catal. Today 41 (1998) 191–206.
[35] E. Kassab, M. Castellà-Ventura, J. Phys. Chem. B 109 (2005) 13716–13728.
[36] M. Castellà-Ventura, Y. Akacem, E. Kassab, J. Phys. Chem C. 112 (2008) 19045–19054.
[37] H. Yasuda, T. Sato, Y. Yoshimura, Catal. Today 50 (1999) 63–71.
[38] M.A. Arribas, A. Martinez, Appl. Catal. A 230 (2002) 203–217.
[39] K. Suzuki, N. Katada, M. Niwa, J. Phys. Chem. C 111 (2007) 894–900.
[40] T. Frising, P. Leflaive, Microporous Mesoporous Mater. 114 (2008) 27–63.
[41] T. Armaroli, E. Finocchio, G. Busca, S. Rossini, Vib. Spectrosc. 20 (1999) 85–94.
[42] E. Karimi, I.F. Texeira, L.P. Ribeiro, A. Gomez, R.M. Lago, G. Penner, S.W. Kycia, M. Schlaf, Catal. Today 190 (2012) 73–88.
[43] O. Nagashima, S. Sato, R. Takahashi, T. Sodesawa, J. Mol. Catal. A 227 (2005) 231–239.
[44] K. Weissermel, H.-J. Arpe, Industrial Organic Chemistry, third completely rev. ed., Wiley-VCH, Weinheim, 1997.
[45] C. Li, P.C. Stair, Catal. Today 33 (1997) 353–360.
[46] R. Kostić, M. Mirić, T. Radić, M. Radović, R. Gajić, Z.V. Popović, Acta Phys. Pol. A 116 (2009) 718–721.
[47] J. Hodkiewicz, Thermo Fisher Scientific, Madison, WI, USA, https://fscimage.thermoscientific.com/images/D19504~.pdf (12.04.13).
[48] P. Castaño, G. Elordi, M. Olazar, A.T. Aguayo, B. Pawelec, J. Bilbao, Appl. Catal. B 104 (2011) 91–100.
[49] F.F. Madeira, K. Ben Tayeb, L. Pinard, H. Vezin, S. Maury, N. Cadran, Appl. Catal. A 443–444 (2012) 171–180.